### Title
Generalized Manning Condensation Model Captures the RNA Ion Atmosphere




### Journal
Physical Review Letters, 114(25)

### ISSN
0031-9007



### Authors
Hayes, Ryan L
Noel, Jeffrey K
Mandic, Ana
et al.



### Publication Date
2015-06-26

### DOI
10.1103/physrevlett.114.258105

Peer reviewed

Published in final edited form as:

*Phys Rev Lett*. 2015 June 26; 114(25): 258105. doi:10.1103/PhysRevLett.114.258105.

# Generalized Manning Condensation Model Captures the RNA Ion Atmosphere

**Ryan L. Hayes**[1], **Jeffrey K. Noel**[1], **Ana Mandic**[2], **Paul C. Whitford**[3], **Karissa Y. Sanbonmatsu**[4], **Udayan Mohanty**[5], and **José N. Onuchic**[1]

[1]Center for Theoretical Biological Physics and Department of Physics & Astronomy, Rice University, Houston, TX

[2]Department of Biomedical Engineering, University of Houston, Houston, TX

[3]Department of Physics, Northeastern University, Boston, MA

[4]Theoretic Biology and Biophysics, Theoretic Division, Los Alamos National Labs, Los Alamos, NM

[5]Department of Chemistry, Boston College, Chestnut Hill, MA

## Abstract

RNA is highly sensitive to the ionic environment, and typically requires $Mg^{2+}$ to form compact structures. There is a need for models capable of describing the ion atmosphere surrounding RNA with quantitative accuracy. We present a model of RNA electrostatics and apply it within coarse-grained molecular dynamics simulation. The model treats $Mg^{2+}$ ions explicitly to account for ion-ion correlations neglected by mean field theories. Since mean-field theories capture KCl well, it is treated implicitly by a generalized Manning counterion condensation model. The model extends Manning condensation to deal with arbitrary RNA conformations, non-limiting KCl concentrations, and the ion inaccessible volume of RNA. The model is tested against experimental measurements of the excess $Mg^{2+}$ associated with the RNA, $\Gamma_{2+}$, because $\Gamma_{2+}$ is directly related to the $Mg^{2+}$-RNA interaction free energy. The excellent agreement with experiment demonstrates the model captures the ionic dependence of the RNA free energy landscape.

RNA is sensitive to the ionic environment because it is strongly negatively charged and yet frequently folds into compact configurations. Such compact configurations require positive counterions to balance RNA charge. $Mg^{2+}$ is especially effective in stabilizing compact configurations as most RNA tertiary structure will not form in the absence of $Mg^{2+}$ [1]. Simplified or coarse-grained molecular dynamics simulations are an ideal tool for studying the molecular details of slow processes in RNA [2–6]; however, their accuracy is limited at present by the lack of accurate and computationally efficient descriptions of the atmosphere of ions associated with RNA. We generalize the theory of Manning counterion condensation [7] to arbitrary geometries and concentrations, making it applicable to compact RNA structures, and show this model accurately represents the ion atmosphere around RNA.

The ubiquity of $Mg^{2+}$ in RNA structure and dynamics arises because $Mg^{2+}$ is small and divalent. The small size of $Mg^{2+}$ allows it to interact more closely with RNA than larger ions [8, 9]. Because $Mg^{2+}$ is divalent, only half as many $Mg^{2+}$ as monovalent ions must be

localized around RNA to balance its charge, allowing twice the entropic cost to be paid per ion [7, 10]. Consequently, $Mg^{2+}$ can outcompete monovalent ions present at much higher concentrations to associate with RNA. The divalence of $Mg^{2+}$ also allows it to induce effective attraction between otherwise repulsive phosphates [10–12]. As a result, $Mg^{2+}$ strongly favors compact RNA conformations [10], and can slow kinetics by raising the free energy of less compact transition states [13]. In many cases, changing $Mg^{2+}$ concentration can switch stability between two conformational basins [14–17]. Electrostatic models capable of describing $Mg^{2+}$-RNA interactions are needed to connect with these experiments and to describe the RNA energy landscape.

The simplest model of electrostatics in ionic solutions is Debye-Hückel electrostatics, in which the ion density is given by the linearized Boltzmann distribution, and dielectric heterogeneity and ion accessibility are neglected. Coarse-grained models of RNA have used a Debye-Hückel treatment of KCl [18, 19]. Such a treatment is not ideal for $Mg^{2+}$ because the linearized Boltzmann distribution is a poor approximation for strong $Mg^{2+}$-RNA interactions near RNA. In addition, Debye-Hückel is unable to produce the effective attraction between phosphates that $Mg^{2+}$ can induce.

Nonlinear Poisson-Boltzmann (NLPB) electrostatics [20–22] removes most of the Debye-Hückel approximations at greater computational expense. NLPB is a mean field treatment, and neglects ion-ion correlations [23, 24] and ion size effects [25–27]. For monovalent ions where these correlations are weak, NLPB performs well, but is less accurate for divalent $Mg^{2+}$ [26, 28]. The tightly bound ion model [24, 29] accounts for ion-ion correlations, and captures the ionic atmosphere well, but is a Monte Carlo technique, and has not yet been adapted for molecular dynamics. Manning counterion condensation theory [7, 30, 31] can describe nonlinear effects near the RNA, but is typically limited to low concentrations and linear or helical RNA geometry.

We recently developed a coarse-grained model with explicit $Mg^{2+}$ and implicit KCl that revealed the importance of accounting for competition between $Mg^{2+}$ and condensed KCl [32]. As a first approximation, KCl condensation was treated as a static function of $Mg^{2+}$ concentration and fit to native basin experimental data. This approximation rendered the model only valid for native basin fluctuations of experimentally characterized RNA. A dynamic, physics-based description of KCl condensation is needed for the model to have any predictive power.

In this letter, we introduce a generalized Manning counterion condensation model that describes folded RNA at physiological ionic concentrations. $Mg^{2+}$ is treated explicitly to account for ion-ion correlations, while KCl condensation is described by the generalized Manning model. We add the electrostatic model to a coarse-grained model of RNA to capture native basin fluctuations. The coarse-grained model is an all heavy atom structure-based model [32–34] with a theoretical base in the energy landscape theory of protein folding [35–37]. The model is in good agreement with experimental measurements of the ion atmosphere within the native basin for several compact RNA molecules at varying KCl and $Mg^{2+}$ concentrations. The model is also applicable beyond the native basin, and the implicit treatment of KCl makes the model computationally inexpensive.

Classical Manning counterion condensation [7] occurs on an infinite line of charge in the low concentration limit due to competition between mixing entropy and electrostatic energy. The mixing free energy per phosphate to condense θ ions per phosphate is given by

$$G_{\mathrm{Mix}}=k_{\mathrm{B}}T\theta\ \ln\ \left(\frac{\theta}{ecV}\right), \quad (1)$$

where $k_{\mathrm{B}}$ is Boltzmann's constant, $T$ is the temperature, $c$ is the bulk concentration of the counterion, $V$ is the volume per phosphate into which the counterions condense, and $e$ is Euler's number. The condensed ions effectively rescale the charge of the phosphates by $1-z\theta$, so the electrostatic energy per phosphate is given by

$$G_{\mathrm{E}}=k_{\mathrm{B}}T(1-z\theta)^2F, \quad (2)$$

where $z$ is the charge of the counterion and $F$ is the Debye-Hückel energy of the bare polyelectrolyte charges per phosphate in units of $k_{\mathrm{B}}T$. For an infinite line of charge at low concentration, $G_{\mathrm{Mix}}$ and $G_{\mathrm{E}}$ (through $F$) both diverge like ln $c$, so the condensation is constant over a wide range of counterion concentrations [7].

Condensation on RNA under physiological conditions differs from classical Manning condensation in two important regards that require the inclusion of additional physics. First, folded RNA is not a line of charge, so $F$ does not diverge like ln $c$, and condensation is not constant over wide concentration ranges. Folded RNA rather forms compact and irregular structures, so a model allowing varying condensation on each phosphate is required to account for the electrostatic heterogeneity of the phosphates. This can be accomplished by making $F$ a dynamical function of phosphate coordinates and adding appropriate phosphate indices to Equations (1) and (2). Second, salts are present at intermediate concentrations. As a result, there is a large population of screening ions near the RNA in addition to the condensed ions that contribute to the mixing free energy. Many of these implicit screening ions occupy the ion inaccessible volume of the RNA and must be removed. Accounting for screening ions and ion inaccessible volume requires more substantial extensions to Manning counterion condensation that we outline below. The resulting generalization of Manning counterion condensation may also have applications in polyelectrolyte theory beyond RNA.

The $K^+$ and $Cl^-$ distributions may be divided into screening ions and Manning condensed ions. The screening ion density is given by a linearized Poisson-Boltzmann distribution, while the condensed ion density captures deviations of the distribution from linearity near RNA. In Debye-Hückel theory, screening ions of species $s$ have a local density

$$n_{\mathrm{DH},s}(\vec{r})=c_s\left(1-\frac{z_s\Phi_0(\vec{r})}{k_{\mathrm{B}}T}\right) \quad (3)$$

that varies linearly with the electrostatic potential $\Phi_0$, where $c_s$ and $z_s$ are the concentration and charge of ionic species $s$. For strong potentials, non-physical negative concentrations are possible, as frequently occurs for $Cl^-$ near RNA. These negative concentrations must be corrected by a corresponding positive concentration of condensed ions. Consequently, it is

necessary to account for both condensed $K^+$ and $Cl^-$ to avoid negative local concentrations of $Cl^-$.

In the present work, the density of Manning condensed ions is modeled as the sum of two normalized Gaussian distributions $P(r, \sigma)$ centered on the position of every RNA charge

$$n_{\mu,s}(\vec{r}) = \sum_i \mu_{is} P(|\vec{r} - \vec{r}_i|, \sigma_\mu) \quad (4)$$

$$n_{\eta,s}(\vec{r}) = \sum_i \eta_{is} P(|\vec{r} - \vec{r}_i|, \sigma_\eta) \quad (5)$$

with charges placed on every phosphate. The total density of ions is then $n_{\mathrm{DH},s} + n_{\mu,s} + n_{\eta,s}$. The mixing Gaussian controls mixing free energy and the size $\sigma_\mu = 0.7$ nm is set to the Bjerrum length. The hole Gaussian enforces the ion accessibility by offsetting any ions too close to the RNA and the size $\sigma_\eta = 0.34$ nm is set approximately to the closest approach of a hydrated ion to RNA. The sensitivity of the results to the two free parameters $\sigma_\mu$ and $\sigma_\eta$ is shown in the supplemental material. The Manning condensed ions of species $s$ at a charged atom $i$ are then given by $\theta_{is} = \mu_{is} + \eta_{is}$. In the model, $K^+$ and $Cl^-$ only condense on phosphates or RNA charges, so $\mu_{is} = \eta_{is} = 0$ at explicit $Mg^{2+}$ charges.

In contrast to the implicit $K^+$ and $Cl^-$ distributions, the $Mg^{2+}$ distribution is determined by the location of the explicit ions. In addition to electrostatic forces, $Mg^{2+}$ ions interact with an $r^{-12}$ excluded volume potential parameterized to keep each $Mg^{2+}$ the fully hexahydrated distance from the RNA and other $Mg^{2+}$ ions [32].

The electrostatic free energy of the RNA and the condensed ions can be given in terms of Debye-Hückel interactions

$$\phi(r_{ij}, 0) = k_{\mathrm{B}} T \frac{l_{\mathrm{B}}}{r_{ij}} \exp(-\kappa r_{ij}) \quad (6)$$

$$\phi(r_{ij}, \sigma) = k_{\mathrm{B}} T \sum_{a=\pm 1} \frac{-1}{2} \frac{l_{\mathrm{B}}}{a r_{ij}} \exp\left(\frac{1}{2}\kappa^2\sigma^2 + \kappa a r_{ij}\right) \times \left(1 - \mathrm{erf}\left(\frac{a r_{ij} + \kappa\sigma^2}{\sigma\sqrt{2}}\right)\right), \quad (7)$$

where $r_{ij}$ is the distance between particles $i$ and $j$, $\kappa$ is the inverse Debye length, and $l_{\mathrm{B}}$ is the Bjerrum length (approximately 7 Å in water at 300 K). The interaction between two point charges is $\varphi(r_{ij}, 0)$, while the interaction between a point and a Gaussian of variance $\sigma^2$ is $\varphi(r_{ij}, \sigma)$, and the interaction between two Gaussians of variance $\sigma_m^2$ and $\sigma_n^2$ is $\phi(r_{ij}, \sqrt{\sigma_m^2 + \sigma_n^2})$. The total electrostatic free energy $G_{\mathrm{E}}$ and electrostatic potential $\Phi$ are then

$$G_{\mathrm{E}} = \frac{1}{2} \sum_{ij} \sum_{mn} q_{m,i} q_{n,j} \phi\left(r_{ij}, \sqrt{\sigma_m^2 + \sigma_n^2}\right) \quad (8)$$

$$\Phi_m(\vec{r}) = \sum_j \sum_n q_{n,j} \phi\left(\vec{r} - \vec{r}_j, \sqrt{{\sigma_m}^2 + {\sigma_n}^2}\right), \quad (9)$$

where the sum on indices $m$ and $n$ runs over the three labels {0, μ, η}, denoting points, mixing Gaussians, and hole Gaussians, respectively; and the sum on $i$ and $j$ runs over all charged atoms including $i = j$ (except when $m = n = 0$) so that condensed ions can interact with their own phosphate. For points, $\sigma_0 = 0$ nm, and $q_{0,i}$ denotes the charge of particle $i$, while the condensed ion charges are $q_{\mu,i} = \sum_s z_s \mu_{is}$ and $q_{\eta,i} = \sum_s z_s \eta_{is}$. The actual potential is $\Phi_0$, while $\Phi_\mu$ and $\Phi_\eta$ are the average of the potential over the Gaussian regions.

At intermediate salt, the mixing free energy in Equation (1) must be reformulated to include screening ions. The substitution $n = \theta / V$ allows the mixing free energy to be expressed in terms of local ion density and condensation volume. The local density $n_{\mathrm{Mix},is}$ can be approximated by averaging $n_{\mathrm{DH},s}$ over the mixing Gaussian, and adding $n_{\mu,s}$

$$n_{\mathrm{Mix,is}} = c_s \left(1 - \frac{z_s \Phi_\mu(\vec{r}_i)}{k_\mathrm{B} T}\right) + n_{\mu,s}(\vec{r}_i). \quad (10)$$

The effective volume a Gaussian occupies can be estimated as the inverse of the local Gaussian density

$$V_{m,i} = 1 / \sum_j P(r_{ij}, \sigma_m), \quad (11)$$

where the sum on $j$ runs over all phosphates. The density of holes $n_{\eta,s}(\vec{r}_i)$ is omitted from Equation (10) because this term serves primarily to make the ion density average to zero within the hole volume $V_{\eta,i}$, consequently this empty volume is subtracted off the mixing volume $V_{\mu,i}$ giving $V_{\mu,i} - V_{\eta,i}$. The mixing free energy is then approximately

$$G_{\mathrm{Mix}} = \sum_i \sum_s k_\mathrm{B} T n_{\mathrm{Mix,is}} \, (V_{\mu,i} - V_{\eta,i}) \, \ln \, (n_{\mathrm{Mix,is}} / e c_s). \quad (12)$$

The potential ensures $n_{\mathrm{Mix},is} \geq 0$, so any nonphysical negative concentration of screening ions will be balanced by a positive concentration of condensed ions.

The electrostatic and mixing free energy of the screening ions are typically ignored because they cancel each other for weak potentials. Since the mixing free energy of the screening ions within the volume $V_{\mu,i} - V_{\eta,i}$ has been included in the free energy, the electrostatic free energy of the screening ions in this region must be included as well. This free energy is given by

$$G_{\mathrm{ES}} = \frac{1}{2} \sum_i \sum_s z_s c_s \left(1 - \frac{z_s \Phi_\mu(\vec{r}_i)}{k_\mathrm{B} T}\right) (V_{\mu,i} - V_{\eta,i}) \Phi_\mu(\vec{r}_i). \quad (13)$$

With generalizations for the electrostatic free energy $G_E$ and mixing free energy $G_{Mix}$ + $G_{ES}$, it is necessary to enforce ion accessibility near the RNA. The concentration of each ionic species $n_{Hole,is}$ within the excluded volume of polyelectrolyte particle $i$ is

$$n_{\mathrm{Hole,is}}=c_s\left(1-\frac{z_s\Phi_\eta(\vec{r}_i)}{k_\mathrm{B}T}\right)+n_{\mu,s}(\vec{r}_i)+n_{\eta,s}(\vec{r}_i), \quad (14)$$

where the screening ions have been averaged over the hole Gaussian. Since ions are excluded from this volume, $n_{Hole,is}$ = 0. Rather than using constraints, a strong harmonic restraint

$$G_{\mathrm{Hole}}=\frac{1}{2}k_{\mathrm{Hole}}\sum_i\sum_s {n_{\mathrm{Hole,is}}}^2 \quad (15)$$

is added to the potential to keep η within 0.01 ions of the correct value. Furthermore, to maintain stability and avoid overfitting the ion distribution, $\mu_{is}$ and $\eta_{is}$ are weakly harmonically restrained to $n_{\mu,s}(\vec{r}_i)V_{\mu,i}$ and $n_{\eta,s}(\vec{r}_i)V_{\eta,i}$, respectively by a term $G_{Rest}$. Together with the $Mg^{2+}$ and RNA positions, the four condensation variables for each phosphate ($\mu_{i+}$, $\mu_{i-}$, $\eta_{i+}$, and $\eta_{i-}$) are treated as coordinates that evolve by Langevin dynamics on the potential $G_E$ + $G_{Mix}$ + $G_{ES}$ + $G_{Hole}$ + $G_{Rest}$. Parameter values and other simulation details may be found in the Supplemental Material.

The ion atmosphere can be quantified by the number of excess ions of each species which associate with an RNA. The number of excess ions of a particular ionic species varies with concentration, but the total charge of all excess ions must balance the RNA charge. At fixed KCl concentration, with $c_+ \gg c_{2+}$, the $Mg^{2+}$-RNA interaction free energy

$$\Delta G_{\mathrm{Mg^{2+}}}=-k_\mathrm{B}T\int_0^{c_{2+}}\Gamma_{2+}d\ \ln\ c'_{2+} \quad (16)$$

is directly related to the excess $Mg^{2+}$, $\Gamma_{2+}$, as a function of $Mg^{2+}$ concentration [38]. $\Gamma_{2+}$ can be measured experimentally with HQS fluorescence [15–17, 38] or other techniques [39], and can be calculated from simulations [32, 40]. Because $\Gamma_{2+}$ bridges between simulation and experiment and is directly related to the $Mg^{2+}$-RNA interaction free energy, it is an ideal quantity for testing models of RNA electrostatics.

The model is able to reproduce $\Gamma_{2+}$ for the adenine riboswitch at 50 mM KCl and for a 58 nucleotide fragment of the ribosome at several KCl concentrations (Figure 1). Experimental data for the adenine riboswitch and ribosomal fragment are taken from reference [15] and [16], respectively. The transferability of the model to several KCl concentrations in Figure 1B bolsters the model, as simpler models lacking RNA excluded volume in Equation (15) can be fit at a single KCl concentration, but break down when applied to multiple KCl concentrations (data not shown). Lower $Mg^{2+}$ concentrations were not explored for the ribosomal fragment because the system undergoes a conformational change we did not wish to model near the inflection point in the experimental data. With further calibration of the underlying coarse-grained model, the generalized Manning condensation model could be used to probe the electrostatic effects driving the conformational transition. The excellent

agreement over a wide range of $Mg^{2+}$ and KCl concentrations suggests the model is capturing the electrostatic free energy quite well.

Native basin fluctuations can have a notable effect on $\Gamma_{2+}$. For the beet western yellow virus pseudoknot the number of excess $Mg^{2+}$ has been measured [17]. In the generalized Manning condensation model, the excess $Mg^{2+}$ is overestimated if the RNA is frozen in the crystal structure, but can be corrected by allowing the RNA to fluctuate (Figure 2). This occurs because the crystal structure contains a negatively charged pocket between the 5' triphosphate tail and the rest of the pseudoknot where $Mg^{2+}$ binds nonspecifically. This pocket is not stable in solution due to phosphate-phosphate repulsion, resulting in accurate $\Gamma_{2+}$ predictions when RNA dynamics are included. The sensitivity of $\Gamma_{2+}$ to small native basin fluctuations reveals the importance of modeling the full conformational ensemble to accurately predict $\Delta G_{Mg^{2+}}$. Sensitivity has been previously observed in partially unfolded ensembles, which exhibit larger fluctuations [16, 17]. Our model is ideally designed to capture these conformational ensembles.

A comparison of the generalized Manning model, NLPB, and previous explicit solvent predictions [40] of $\Gamma_{2+}$ for the SAM-I riboswitch is shown in the supplemental material. Explicit solvent simulations appear to underpredict $\Gamma_{2+}$, possibly because $K^+$ can dehydrate too easily [41] and drive away $Mg^{2+}$. Many ion parameters have been proposed for explicit solvent simulation [42–45]. The excess $Mg^{2+}$ is a sensitive measure of RNA electrostatics that may be useful in future calibration of explicit solvent ion parameters.

The generalized Manning model provides a more accurate description of the ion atmosphere than the conventional descriptions of Debye-Hückel, nonlinear Poisson-Boltzmann equation, classical Manning counterion condensation, and possibly even explicit solvent simulation. This success is due in part to the explicit treatment of $Mg^{2+}$ that accounts for ion-ion correlations [24] absent from mean field treatments. The implicit treatment of KCl makes the model computationally inexpensive, both by significantly reducing the number of particles in the large boxes required for a bath of free $Mg^{2+}$, and by allowing the use of the short range Debye-Hückel potential rather than the long range Coulomb potential.

Our previous model of RNA electrostatics served as a valuable proof of concept: $\Gamma_{2+}$ can be predicted correctly by accounting for KCl condensation [32]. In that model, KCl condensation was treated as an experimentally fit function of $Mg^{2+}$ concentration that was static within a simulation, but this approximation introduced extensive limitations that made the model untransferable and unusable for dynamics. The fit to experimental meant the model could only be used on RNA systems at specific KCl concentrations where $\Gamma_{2+}$ had been measured. The assumption of static KCl condensation confined one to a single conformational basin where KCl condensation does not change and introduced inconsistencies that undermine Equation (16).

The model presented in this letter removes all of these limitations by making KCl condensation a dynamical quantity dependent on atomic coordinates and calculated from physical principles. Since the potential is in terms of atomic coordinates and KCl condensation, it is transferable, phosphate-phosphate repulsion is automatically included,

and KCl condensation can respond to conformational changes, making the model applicable beyond the native basin. Consequently, this model provides a description of the electrostatic features of the full RNA free energy landscape, and allows calculation of $\Delta\Delta G_{Mg^{2+}}$ between conformational basins. The electrostatic description is in a dynamic context which can access long time scales inaccessible with other techniques and connect with experiments.

See Supplemental Material at [URL] for comparison with explicit solvent simulations, parameter sensitivity analysis, and further details of the model. The parallel code used to simulate the potential is available for download at http://smog.rice.edu/SBMextension.html.

## Supplementary Material

Refer to Web version on PubMed Central for supplementary material.

## Acknowledgments

Work at the Center for Theoretical Biological Physics was sponsored by the NSF (Grants PHY-1427654 and MCB-1214457) and by the Welch Foundation Grant No. C-1792. A.M. was supported by the NSF (Grant PHY-1216435). P.C.W. was supported by an NSF CAREER Award (Grant MCB-1350312). K.Y.S. support was provided by the National Institutes of Health. U.M. is a John Simon Guggenheim Memorial Foundation fellow. J.N.O. is a CPRIT Scholar in Cancer Research sponsored by the Cancer Prevention and Research Institute of Texas. Computing resources were provided by Rice University and supported in part by the Cyberinfrastructure for Computational Research funded by NSF under Grant CNS-0821727.

## References

1. Draper DE. RNA: A Publication of the RNA Society. 2004; 10:335.
2. Hyeon C, Denesyuk NA, Thirumalai D. Israel Journal of Chemistry. 2014; 54:1358.
3. Lin J-C, Thirumalai D. Journal of the American Chemical Society. 2013; 135:16641. [PubMed: 24087850]
4. Whitford PC, Geggier P, Altman RB, Blanchard SC, Onuchic JN, Sanbonmatsu KY. RNA: A Publication of the RNA Society. 2010; 16:1196.
5. Lutz B, Faber M, Verma A, Klumpp S, Schug A. Nucleic Acids Research. 2014; 42:2687. [PubMed: 24275497]
6. Mustoe AM, Al-Hashimi HM, Brooks CL III. Journal of Physical Chemistry B. 2014; 118:2615.
7. Manning GS. Quarterly Reviews of Biophysics. 1978; 11:179. [PubMed: 353876]
8. Lambert D, Leipply D, Shiman R, Draper DE. Journal of Molecular Biology. 2009; 390:791. [PubMed: 19427322]
9. Koculi E, Hyeon C, Thirumalai D, Woodson SA. Journal of the American Chemical Society. 2007; 129:2676. [PubMed: 17295487]
10. Heilman-Miller SL, Thirumalai D, Woodson SA. Journal of Molecular Biology. 2001; 306:1157. [PubMed: 11237624]
11. Thirumalai, D.; Hyeon, C. Chapter 2: Theory of RNA Folding: From Hairpins to Ribozymes. W, NG., editor. Springer Berlin Heidelberg; 2009. p. 27-47.
12. Wittmer J, Johner A, Joanny JF. Journal de Physique II. 1995; 5:635.
13. Heilman-Miller SL, Pan J, Thirumalai D, Woodson SA. Journal of Molecular Biology. 2001; 309:57. [PubMed: 11491301]
14. Hennelly SP, Novikova IV, Sanbonmatsu KY. Nucleic Acids Research. 2013; 41:1922. [PubMed: 23258703]
15. Leipply D, Draper DE. Biochemistry. 2011; 50:2790. [PubMed: 21361309]
16. Grilley D, Misra V, Caliskan G, Draper DE. Biochemistry. 2007; 46:10266. [PubMed: 17705557]
17. Soto AM, Misra V, Draper DE. Biochemistry. 2007; 46:2973. [PubMed: 17315982]

18. Hyeon C, Thirumalai D. Proceedings of the National Academy of Sciences of the United States of America. 2005; 102:6789. [PubMed: 15749822]
19. Cho SS, Pincus DL, Thirumalai D. Proceedings of the National Academy of Sciences of the United States of America. 2009; 106:17349. [PubMed: 19805055]
20. Honig B, Nicholls A. Science. 1995; 268:1144. [PubMed: 7761829]
21. Chen SW, Honig B. Journal of Physical Chemistry B. 1997; 101:9113.
22. Baker NA, Sept D, Joseph S, Holst MJ, McCammon JA. Proceedings of the National Academy of Sciences of the United States of America. 2001; 98:10037. [PubMed: 11517324]
23. Chen, AA.; Marucho, M.; Baker, NA.; Pappu, RV. Biophysical, Chemical, and Functional Probes of RNA Structure, Interactions and Folding: Part B, Methods in Enzymology. Herschlag, D., editor. Vol. 469. Academic Press; 2009. p. 411-432.
24. He Z, Chen S-J. Journal of Chemical Theory and Computation. 2012; 8:2095. [PubMed: 23002389]
25. Boschitsch AH, Danilov PV. Journal of Computational Chemistry. 2012; 33:1152. [PubMed: 22370918]
26. Chu VB, Bai Y, Lipfert J, Herschlag D, Doniach S. Biophysical Journal. 2007; 93:3202. [PubMed: 17604318]
27. Borukhov I, Andelman D. Physical Review Letters. 1997; 79:435.
28. Lipfert J, Doniach S, Das R, Herschlag D. Annual Review of Biochemistry. 2014; 83:813.
29. Chena G, Tana Z-J, Chen S-J. Biophysical Journal. 2010; 98:111. [PubMed: 20085723]
30. Manning GS. Biophysical Chemistry. 2002; 101:461. [PubMed: 12488020]
31. Denesyuk NA, Thirumalai D. Journal of Physical Chemistry B. 2013; 117:4901.
32. Hayes RL, Noel JK, Whitford PC, Mohanty U, Sanbonmatsu KY, Onuchic JN. Biophysical Journal. 2014; 106:1508. [PubMed: 24703312]
33. Whitford PC, Noel JK, Gosavi S, Schug A, Sanbonmatsu KY, Onuchic JN. Proteins: Structure, Function, and Bioinformatics. 2009; 75:430.
34. Whitford PC, Schug A, Saunders J, Hennelly SP, Onuchic JN. Biophysical Journal. 2009; 96:L7. [PubMed: 19167285]
35. Onuchic JN, Luthey-Schulten Z, Wolynes PG. Annual Review of Physical Chemistry. 1997; 48:545.
36. Zwanzig R, Szabo A, Bagchi B. Proceedings of the National Academy of Sciences of the United States of America. 1992; 89:20. [PubMed: 1729690]
37. Bryngelson JD, Wolynes PG. Proceedings of the National Academy of Sciences of the United States of America. 1987; 84:7524. [PubMed: 3478708]
38. Grilley D, Soto AM, Draper DE. Proceedings of the National Academy of Sciences of the United States of America. 2006; 103:14003. [PubMed: 16966612]
39. Bai Y, Greenfeld M, Travers KJ, Chu VB, Lipfert J, Doniach S, Herschlag D. Journal of the American Chemical Society. 2007; 129:14981. [PubMed: 17990882]
40. Hayes RL, Noel JK, Mohanty U, Whitford PC, Hennelly SP, Onuchic JN, Sanbonmatsu KY. Journal of the American Chemical Society. 2012; 134:12043. [PubMed: 22612276]
41. Braunlin, WH. Advances in Biophysical Chemistry, Advances in Biophysical Chemistry. Vol. 5. JAI Press; 1995. p. 89-139.
42. Dang LX. Journal of the American Chemical Society. 1995; 117:6954.
43. Chen AA, Pappu RV. Journal of Physical Chemistry B. 2007; 111:11884.
44. Allnér O, Nilsson L, Villa A. Journal of Chemical Theory and Computation. 2012; 8:1493. [PubMed: 26596759]
45. Saxena A, García AE. Journal of Physical Chemistry B. 2015; 119:219.

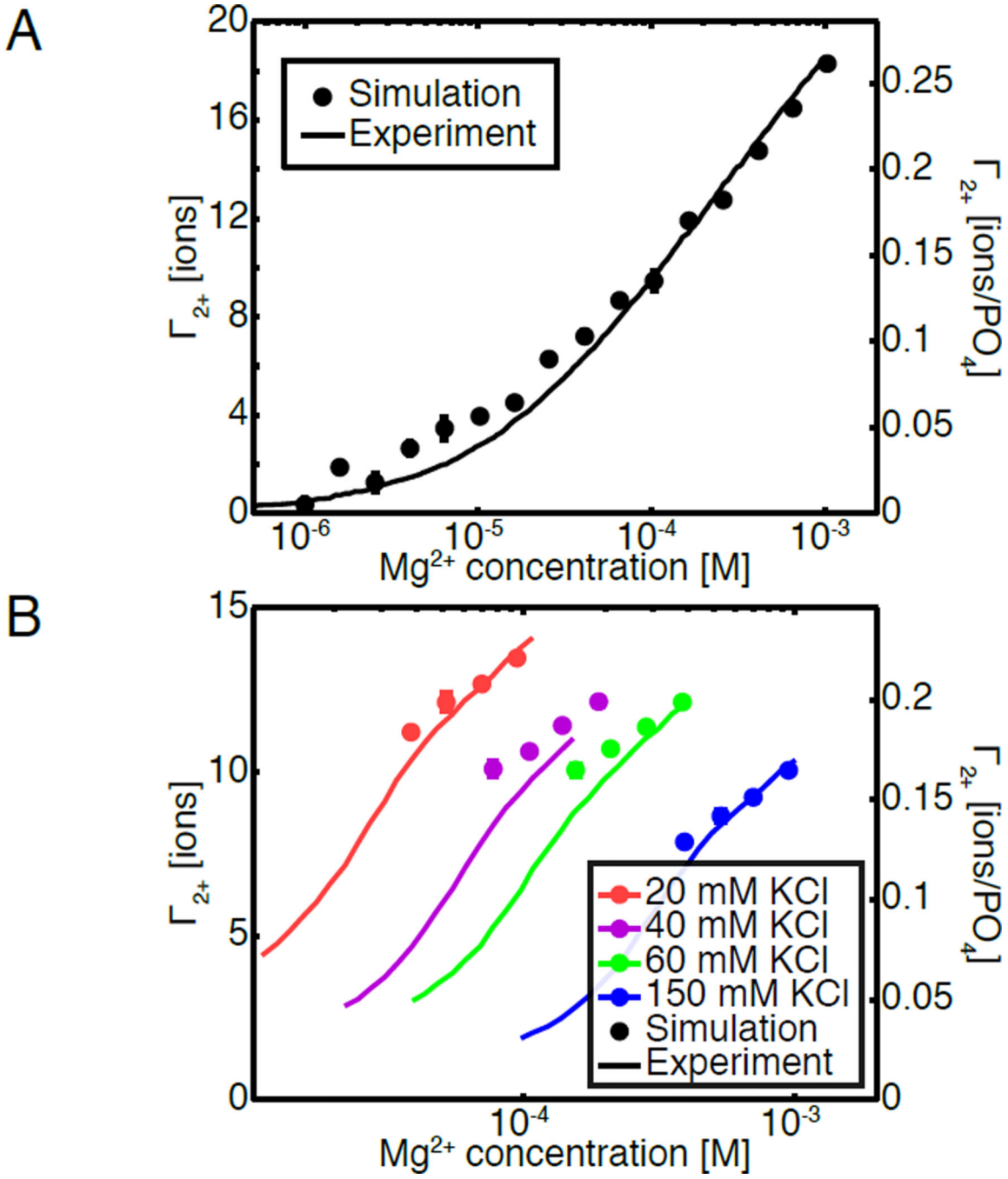


**FIG. 1.**

The model captures excess $Mg^{2+}$ over a wide range of concentrations for both (A) the adenine riboswitch at 50 mM KCl, and (B) a 58 nucleotide ribosomal fragment. Experimental results are plotted as lines and simulation results are plotted as dots.

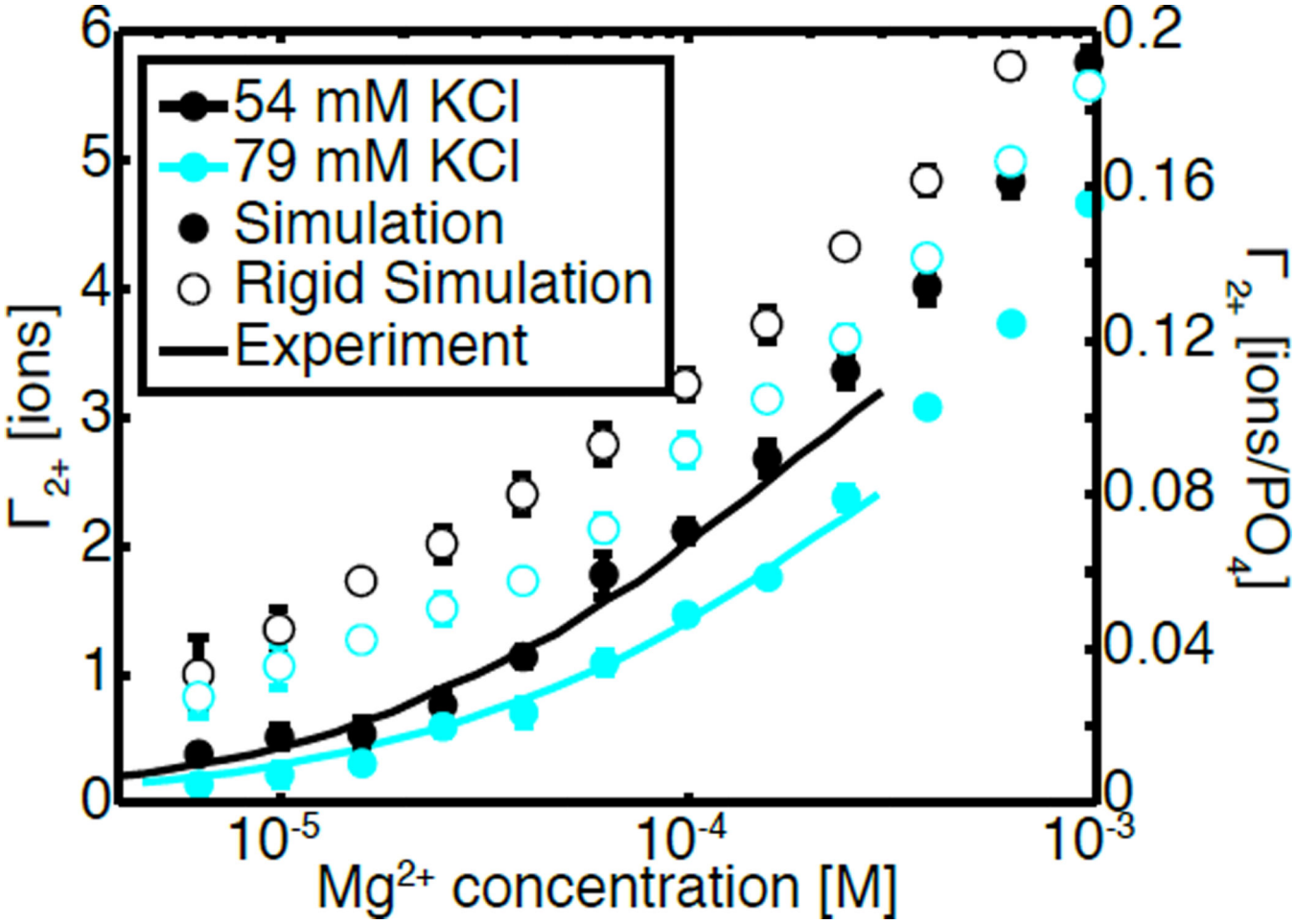


**FIG. 2.**

Predictions of the model are too high for the beet western yellow virus pseudoknot in the rigid simulation where the RNA is fixed in the crystal structure (open circles). The agreement with experiment is quite close if native basin fluctuations are included (solid circles).